International Journal of Refrigeration 142 (2022) 92–102

Contents lists available at ScienceDirect

International Journal of Refrigeration

journal homepage: www.elsevier.com/locate/ijrefrig

Experimental and numerical study of dew-point indirect evaporative coolers to optimize performance and design

Étude expérimentale et numérique des refroidisseurs évaporatifs indirects au point de rosée pour optimiser les performances et la conception

Francisco Comino [a,*], María Jesús Romero-Lara [b], Manuel Ruiz de Adana [b]

[a] *Departamento de Mecánica, Escuela Politécnica Superior, Universidad de Córdoba, Campus de Rabanales, Antigua Carretera Nacional IV, km 396, Córdoba, 14071 España*

[b] *Departamento de Química-Física y Termodinámica Aplicada, Escuela Politécnica Superior, Universidad de Córdoba, Campus de Rabanales, Antigua Carretera Nacional IV, km 396, Córdoba, 14071 España*

ARTICLE INFO

Keywords:
Dew-point effectiveness
Coefficient of performance
Air-cooling system

Mots clés:
Efficacité au point de rosée
Coefficient de performance
Système de refroidissement de l'air

ABSTRACT

Dew-point indirect evaporative coolers (DIEC) allow to significantly reduce air temperature from supply air flow and require a low energy consumption, so they could be an interesting alternative to conventional air-cooling system. In the present work, the optimal geometric design and the optimal operational parameters of DIEC systems to achieve cooling conditions and comply with the European ventilation regulations were determined. Hence, the experimental energy performance of a DIEC under different inlet air conditions was studied, and a detailed DIEC model based on the ε-NTU method was developed and validated. The experimental results showed very high DIEC dew-point effectiveness values, up to 0.87. Additionally, the numerical results obtained with the detailed DIEC model were in very good agreement with the experimental results, so this model can be adequately used to analyse and optimise DIEC systems. The optimal geometric designs and operational parameters of the DIEC systems depended on the type of space to be conditioned and the ventilation category. The maximum COP values were always obtained for low values of volumetric air flow rate, 50.26 for an office application, 44.19 for the restaurant application and 37.14 for the auditorium application. However, the highest compactness of the DIEC designs were achieved for medium and high values of volumetric air flow rate ratio, between 0.45 and 0.8. The results obtained could significantly help to achieve the objectives of sustainable cooling and ventilation of spaces in the frame of Nearly Zero Energy Buildings.

1. Introduction

The growing global demand for cooling in buildings and industry leads to an increase in energy consumption (IEA, 2018). Indirect evaporative cooling, IEC, technology is an efficient technique for cooling applications and presents an alternative solution to refrigeration vapour compression technology, commonly used for cooling and indoor air temperature control in buildings. In IEC systems, the process air stream is cooled at constant humidity, which is crossed by a secondary air stream humidified with water (Comino et al., 2018a, 2018b).

The IEC systems can be designed in a variety of configurations: "classic" cross-flow exchanger, "classical" counter-flow exchanger, regenerative exchanger, multi-perforated regenerative exchanger, etc. (Pandelidis et al., 2017). One of the most effective indirect evaporative cooling solutions are the dew-point counter-flow cycles (Sadighi Dizaji et al., 2018a), such as Maisotsenko IEC (MIEC). DIEC systems have been studied for many applications, such as pre-cooling of a gas turbine (Sadighi Dizaji et al., 2019), pre-cooling of a compressor (Sohani et al., 2017) or combined with desiccant systems (Romero-lara et al., 2021). Moreover, these systems cool air using 100% outside air, thus handling thermal loads in a space and improving indoor air quality. Therefore, DIEC could be an adequate solution to reduce airborne transmission risk related to respiratory viruses in buildings (Wang et al., 2021).

The thermal performance of IEC systems has been studied under different inlet conditions in previous research works (Comino et al.,

* Corresponding author.
E-mail address: francisco.comino@uco.es (F. Comino).

https://doi.org/10.1016/j.ijrefrig.2022.06.006
Received 20 January 2022; Received in revised form 11 May 2022; Accepted 2 June 2022
Available online 3 June 2022

Nomenclature

A	area [m^2]
b	channel height [m]
$\dot{C}$	heat capacity rate [kg s^{-1}]
C_{DIEC}	compactness of dew-point indirect evaporative cooler [W m^{-3}]
$CO_{2,ind}$	indoor carbon dioxide [ppm]
cp	specific heat capacity [kJ kg^{-1} K^{-1}]
D	hydraulic diameter [m]
e	channel width [m]
f	friction factor
h	specific enthalpy [kJ kg^{-1}]
H	height of the exchanger [m]
k	thermal conductivity [W m^{-1} K^{-1}]
L	length of the exchanger [m]
$\dot{m}$	mass air flow rate [kg s^{-1}]
N1-N50	experimental tests
$N_{channels}$	number of channels
Nu	Nusselt's number
$\dot{Q}$	heat transfer rate [W]
R	ratio of volumetric air flow rate
Re	Reynolds number
RH	relative humidity [%]
T	temperature [C]
U	overall heat transfer coefficient [W m^{-2} K^{-1}]
v	air velocity [m s^{-1}]
$\dot{V}$	volumetric air flow rate [m^3 h^{-1}]
Vol	volume [m^3]
W	width of the exchanger [m]
$\dot{W}$	electric energy consumption [W]
X	distance of sub-heat exchanger [m]
z	slope of the temperature-enthalpy saturation line [kJ kg^{-1} K^{-1}]

Greek letters

α_c	convective heat transfer coefficients [W m^{-2} K^{-1}]
α_m	mass transfer coefficient between working air and water film [kg m^{-2} s^{-1}]
ΔP	total pressure drop [Pa]
ΔT	temperature increase [C]
β	mass transfer coefficient for water vapour [kg s^{-1} m^{-2}]
δ	thickness of plates [m]
ε	effectiveness
η	efficiency
μ	dynamic viscosity [kg m^{-1} s^{-1}]
ρ	density [kg m^{-3}]
σ	surface wetting factor
τ	minor loss coefficient
ω	humidity ratio [kg^{-1}]

Subscripts

cool	cool
DIEC	dew-point indirect evaporative cooler
dp	dew point
EA	exhaust air
f	friction loss
i	number of sub-heat exchanger
in	inlet
m	minor loss
p	primary
out	outlet
RA	return air
s	secondary
sat	saturated
SA	supply air

Acronyms

AHU	air handling unit
CC	cooling coil
COP	coefficient of performance
DIEC	dew-point indirect evaporative cooler
EES	engineering equation solver
F	fan
HC	heating coil
IEC	indirect evaporative cooler
MIEC	Maisotsenko indirect evaporative cooler
NTU	number of transfer units
SH	steam humidifier

2020; Guilizzoni et al., 2019; Jafarian et al., 2017; Sohani et al., 2016). The outlet air conditions and performance of a DIEC were analysed experimentally and numerically (Lin et al., 2018). The supply air temperature ranged between 15.9 and 23.3 °C, with a COP of between 8.6 and 27. A research work on the performance of a DIEC showed that the cooling capacity of the system was significantly reduced when the inlet air humidity ratio was high (Lin et al., 2017). To address this problem, an air dehumidification process prior to the air-cooling process was proposed, improving the cooling capacity by up to 70%. Other study analysed experimentally a MIEC in order to develop a mathematical model of this system (Pandelidis and Anisimov, 2016). This study presented that the most influential input parameters on the system performance were inlet air temperature, inlet air relative humidity and supply air flow rate. These authors also numerically analysed an MIEC system under moist inlet air conditions (Pandelidis et al., 2020). The results of this work showed that the system allowed to reduce the outlet air temperature below the dew point temperature, using the exhaust airflow of a building as secondary air stream of MIEC. An experimental installation with three channels (one primary and two secondary channel) was built to analyse different IEC configurations (Shahzad et al., 2019). The results showed that the vertical heat exchanger configuration was optimal for water distribution. The COP values of this system ranged between 37 and 78.

Some geometric parameters of DIEC systems have also been analysed in recent works in order to improve their thermal behaviour. The cooling capacity of a DIEC system with different number of perforations between the primary and secondary channels was numerically analysed (Oh et al., 2019). The results showed that the configuration with single perforation achieved 10% more cooling capacity than two configurations with four perforations. Other authors developed a mathematical model of MIEC to investigate its behaviour with different numbers of perforations (Sadighi Dizaji et al., 2018b). Two DIEC with cross flow configuration, one with fins and one without fins, were developed and analysed experimentally under different inlet air conditions (Ali et al., 2020). The DIEC system with fins improved thermal performance up to 37% compared to the same system without fins. Other authors analysed the humidification system of the secondary channels of a DIEC (Shahzad et al., 2021). The coefficient of performance and efficiency of the air-cooling system was 45 and 80%, respectively.

Usually, DIEC units have been studied for mild climatic conditions or as a pre-cooling system. However, the cooling and ventilation potential of this technology could allow a quantitative leap in the energy efficiency of air-cooling systems compared to conventional systems based on direct expansion units. Therefore, the main novelty of this work was

to evaluate and optimize the performance and design of DIEC units to cool and ventilate different types of buildings according to the European Building Ventilation Standards.

The main objective of this work was to determine the optimal geometric design and the optimal operational parameters of a DIEC to be able to achieve cooling conditions and comply with the European ventilation regulations (EN-16798–1, 2019). To obtain this, two secondary objectives were carried out: first, to experimental study of the energy behaviour of the DIEC under different inlet air conditions, and then to develop and validate a detailed DIEC model based on the ε-NTU method.

2. Methodology

2.1. Experimental setup

In order to analyse DIEC performance under different working conditions, a test facility has been built. A schematic diagram of the DIEC experimental setup is shown in Fig. 1. The inlet air temperature, relative humidity and air flow rate of process stream were set using an AHU. The main technical characteristic of the experimental setup were described in a previous work of the authors (Comino et al., 2019).

The DIEC system consisted of a counter-flow heat and mass exchanger, a water storage system at the top, a hydraulic pump and an outer casing. The heat and mass exchanger was manufactured of polymer sheets coated with hydrophilic material on one side to retain water. These sheets were stacked alternately and joined together to create multiple air channels on the dry side and on the wet side. The heat exchanger was designed with three water inlets at the top of each secondary air channel and three water passages at the bottom of the secondary channels to allow the removal of excess water. The main technical characteristic of the DIEC are summarized in Table 1.

The data of temperature, humidity and air flow rate were measured and recorded for each experimental test. The sensor locations are shown in Fig. 1. The measured variables in the test rig, the type of sensor and its accuracy are shown in Table 2. The sampling time was 5 s and the values were averaged every 20 min.

2.2. Performance indexes of dew-point indirect evaporative cooler

The experimental thermal behaviour of the DIEC was studied in terms of variation of process air temperature, ΔT, and dew point effectiveness, ε_{dp}. These performance indexes were expressed by Eqs. (1) and (2), respectively.

$$\Delta T = T_{in} - T_{SA} \tag{1}$$

Table 1
Technical characteristics of the dew-point indirect evaporative cooler.

Description	Parameter	Value
Plates material		PVC film with hydrophilic material
Width of the exchanger	W	1.175 m
Length of the exchanger	L	1.2 m
Height of the exchanger	H	0.75 m
Channel width	e	3.4 mm
Channel height	b	80 mm
Thickness of plates	δ	0.48 mm
Nominal inlet volumetric flow rate	$\dot{V}_{in}$	5000 $m^3\,h^{-1}$

Table 2
Technical specification of measuring devices.

Parameter	Type of sensor	Accuracy
T	PT100	±0.2 °C (between 0 °C and 50 °C)
RH	Capacitive	±3% (between 0 and 90%)
$\dot{V}$	Differential pressure transmitter	±5% (at range < 500 Pa)

$$\varepsilon_{dp} = \frac{T_{in} - T_{SA}}{T_{in} - T_{dp,SA}} \tag{2}$$

The DIEC experimental tests were carried out under different air conditions, see in Table 3. The input variables were T_{in}, ω_{in}, $\dot{V}_{in}$, and R, see Eq. (3). The tests N1-N21 were used to evaluate ΔT and ε_{dp}. On the other hand, the tests N1-N50 were used to validate a detailed DIEC mathematical model. A wide range of input conditions were experimentally tested to validate the developed mathematical model. These ranges allowed the use of the mathematical model under different climatic conditions. T_{in} was varied from 32 °C to 43 °C, ω_{in} was varied from 6 g kg^{-1} to 13 g kg^{-1}, $\dot{V}_{in}$ was varied from 3000 $m^3\,h^{-1}$ to 4500 $m^3\,h^{-1}$ and R was varied from 0.2 to 0.8.

$$R = \frac{\dot{V}_{EA}}{\dot{V}_{in}} \tag{3}$$

2.3. Detailed dew-point indirect evaporative cooler model

A detailed mathematical model of DIEC has been developed. The DIEC model was based on the effectiveness (ε) and the Number of Transfer Units (NTU) method, usually used to calculate the rate of heat transfer in heat exchangers. The developed model was modified to also take into account the wet surface fraction of the return air channels of

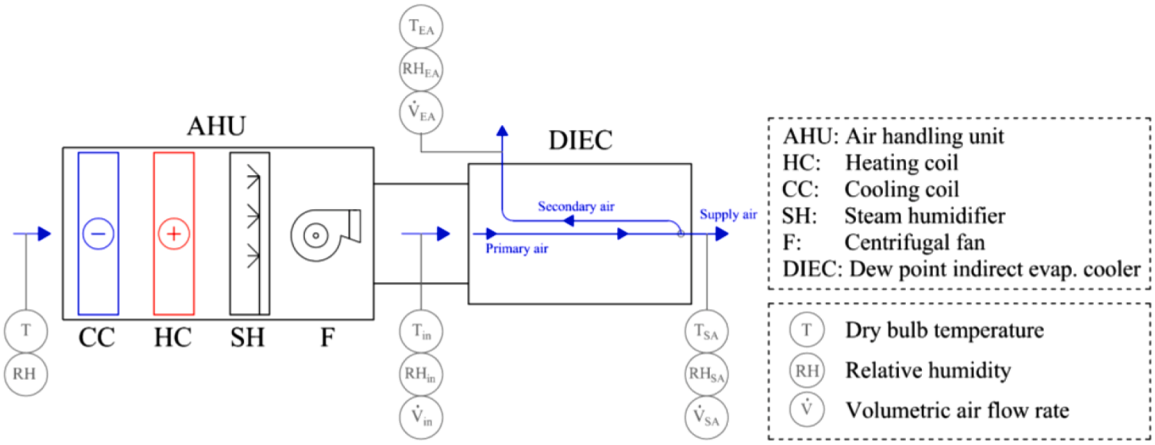

Fig 1. Layout of the test facility of the dew-point indirect evaporative cooler.

Table 3
Experimental tests.

Test	T_{in}[°C]	ω_{in}[g kg^{-1}]	$\dot{V}_{in}$[m^3 h^{-1}]	R[-]	Test	T_{in}[°C]	ω_{in}[g kg^{-1}]	$\dot{V}_{in}$[m^3 h^{-1}]	R[-]
N1	32	6	3500	0.2	N28	33	9.2	4000	0.3
N2	32	6	3500	0.3	N29	33	9.2	4000	0.4
N3	32	6	3500	0.4	N30	33	9.2	4000	0.5
N4	32	6	3500	0.5	N31	43	9.2	4000	0.3
N5	32	6	3500	0.6	N32	43	9.2	4000	0.4
N6	32	6	3500	0.7	N33	43	9.2	4000	0.5
N7	32	6	3500	0.8	N34	41	9.2	4400	0.3
N8	42	6	3500	0.2	N35	41	9.2	4400	0.4
N9	42	6	3500	0.3	N36	41	9.2	4400	0.5
N10	42	6	3500	0.4	N37	41	9.2	3400	0.3
N11	42	6	3500	0.5	N38	41	9.2	3400	0.4
N12	42	6	3500	0.6	N39	41	9.2	3400	0.5
N13	42	6	3500	0.7	N40	37.5	10	4200	0.5
N14	42	6	3500	0.8	N41	37.5	10	4200	0.35
N15	42	6	4500	0.2	N42	37.5	10	4100	0.7
N16	42	6	4500	0.3	N43	37.5	8.7	3400	0.3
N17	42	6	4500	0.4	N44	37.5	8.7	3400	0.35
N18	42	6	4500	0.5	N45	37.5	8.7	3400	0.45
N19	42	6	4500	0.6	N46	33	9	3400	0.3
N20	42	6	4500	0.7	N47	33	9	3400	0.35
N21	42	6	4500	0.8	N48	33	9	3400	0.45
N22	39	13	3000	0.3	N49	39	12.6	4200	0.35
N23	41	13	3000	0.4	N50	39	12.6	4200	0.65

the heat exchanger. Similar detailed DIEC models have been investigated in previous research work (Duan et al., 2017; Hasan, 2012). Therefore, a brief description of the model is reported in the present research.

Main adopted assumptions of the heat exchanger were: (i) No heat losses to the surroundings; (ii) Negligible heat conduction along heat exchanger plates; (iii) Air conditions and heat and mass transfer coefficients are uniform inside each sub-heat exchanger; (iv) Reynolds analogy between heat and mass transfer is valid and Le=1; (v) Negligible resistance to heat transfer in the air-water interface, so that the interface temperature is saturated at the water film temperature.

The ε-NTU solution can be individually applied to n sub-heat exchangers of a DIEC, see Fig. 2. For this study, 100 sub-heat exchangers were considered. The governing equations applied to the primary air stream (p), to the secondary air stream (s) and to the surface of the heat exchanger are defined through the following equations.

The total heat transfer rate was computed with energy balance on the primary-side fluid:

$$\dot{Q}_T = \dot{m}_p \cdot \left(h_{p,out} - h_{p,in}\right) \tag{4}$$

The air conditions of the primary-side and secondary-side fluids entering and leaving each sub-heat exchanger were also obtained by an energy balance, see Eqs. (5) and (6).

$$\dot{Q}_i = \dot{m}_p \cdot \left(h_{p,i} - h_{p,i-1}\right) \tag{5}$$

$$\dot{Q}_i = \dot{m}_s \cdot \left(h_{s,i+1} - h_{s,i}\right) \tag{6}$$

The outlet thermal conditions of the air flow in primary channels were equal to the inlet thermal conditions of air flow in secondary channels for the DIEC. The air humidity ratio in primary channels were constant. The air humidity ratio in the secondary channels, before reaching saturation conditions, was calculated through a mass balance, see Eq. (7)

$$\dot{m}_s \cdot \left(\omega_{s,i} - \omega_{s,i+1}\right) = \beta_i \cdot A_i \cdot \left(\omega_{sat,i} - \omega_{s,i}\right) \tag{7}$$

Where $\omega_{sat,i}$ is the saturated humidity ratio at water temperature; β_i is the mass transfer coefficient for water vapour from the water film to the air stream, Eq (8).

$$\beta_i = \alpha_{m,i} \cdot \sigma \tag{8}$$

The surface wetting factor (σ) was considered constant (0.8) Ren and Yang, 2006). The mass transfer coefficient between working air and water film ($\alpha_{m,i}$) has been calculated by Eq (9), and the local convective heat transfer coefficients (α_c) by Eqs. (10) and ((11).

$$\alpha_{m,i} = \frac{\alpha_{c,s,i}}{cp_{c,i}} \tag{9}$$

$$\alpha_{c,p,i} = \frac{Nu_{p,i} \cdot k_{p,i}}{D} \tag{10}$$

$$\alpha_{c,s,i} = \frac{Nu_{s,i} \cdot k_{s,i}}{D} \tag{11}$$

Where cp is the specific heat capacity; k is the air thermal conductivity; D is the hydraulic diameter of the channels; Nu is the Nusselt's number. Nu was calculated through the EES model Ductflow_n_local Klein, 2020), which depends on Reynold's number (Eqs. (12) and ((13)), Prandtl number,x_i/D, aspect ratio and relative roughness.

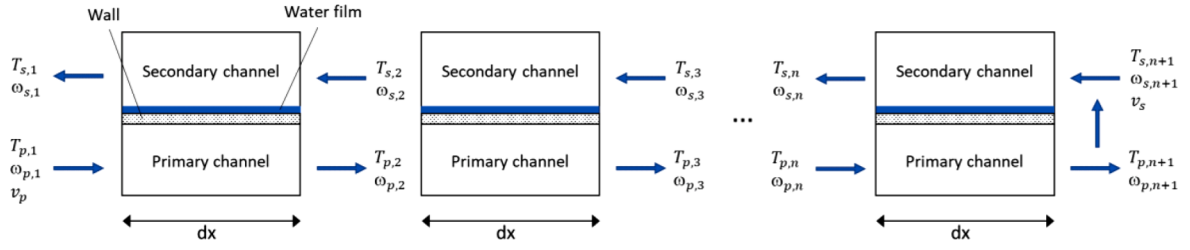

Fig 2. Sub-heat exchangers of a dew-point indirect evaporative cooler.

$$\mathrm{Re}_{pi} = v_p \frac{p_{pi} D}{\mu_{pi}} \tag{12}$$

$$Re_{s,i} = v_s \frac{p_{s,i} D}{m_{s,i}} \tag{13}$$

The air velocities in the primary and secondary channels were obtained by Eqs. (14) and (15), respectively.

$$v_p = \frac{m_p p_{p,i}}{0.5 W b N_{channels}} \tag{14}$$

$$v_s = \frac{m_s p_{s,i}}{0.5 W b N_{channels}} \tag{15}$$

The heat capacity rates on primary-side and secondary-side within each sub-heat exchanger were defined by Eqs. (16) and (17).

$$C_{p,i} = m_p \frac{cp_{p,i}}{z_i} \tag{16}$$

$$C_{s,i} = m_s \tag{17}$$

Where z is the slope of the temperature-enthalpy saturation line, see Eq. (18).

$$z_i = \frac{h_{sat,i} - h_{sat,i+1}}{T_{p,i} - T_{p,i+1}} \tag{18}$$

The effectiveness of each sub-heat exchanger was computed by Eq. (19). The maximum possible heat transfer rate was the product of the minimum value of $\dot{C}_{p,i}$ and $\dot{C}_{s,i}$ and the maximum enthalpy difference.

$$\varepsilon_i = \frac{\mathrm{Q}}{MIN\left(C_{pi}, C_{s,i}\right)\left(h_{sat,i} - h_{sat,i+1}\right)} \tag{19}$$

The number of transfer units required by each sub-heat exchanger (NTU_i) was obtained using the ε-NTU solution for a counter-flow heat exchanger, implemented by the function HX in EES software (Klein, 2020). The conductance required in each sub-heat exchanger was obtained by Eq. (20).

$$U_i A_i = NTU_i MIN\left(C_{p,i} C_{s,i}\right) \tag{20}$$

The overall heat transfer coefficient (U_i) was expressed in Eq. (21).

$$U = \frac{1}{z_i\left[\frac{1}{\alpha_{cpi}} + \frac{\delta}{k_{wall}} + \frac{\delta}{k_{water}}\right] + \frac{1}{\beta_i}} \tag{21}$$

The values of thermal conductivity of wall (k_{wall}) and of thermal conductivity of water film (k_{water}) and thickness of water film (δ_{water}) were considered equal to 0.53 W m^{-1} K^{-1}, 0.3 W m^{-1} K^{-1} and 0.3 mm, respectively.

The energy consumption of a fan to overcome the load drops of the heat exchanger was calculated by Eq. (23).

$$W = \frac{\Delta P_p V_p + \Delta P_s V_s + \Delta P_{SA} V_{SA}}{\eta} \tag{23}$$

Where ΔP is the total pressure drop (friction loss, ΔP_f, and minor loss, ΔP_m); η is the fan efficiency. Each ΔP was obtained by Eq. (24).

$$\Delta P = \Delta P_f + \Delta P_m = f \frac{p v^2}{2D} + \sum \tau \frac{p v^2}{2} \tag{24}$$

The numerical DIEC model was implemented in EES software (Klein, 2020). This model allowed to predict the outlet air conditions or obtain the length of the heat exchanger from pre-established inlet and outlet air conditions.

2.4. Optimization of the dew-point indirect evaporative cooling system

In the present work, the optimal geometric design and the optimal operational parameters of DIEC to be able to achieve cooling conditions and comply with the European ventilation regulations (EN-16798–1, 2019) were studied. Three case studies were carried out for this analysis. The first case study was related to an office application, the second one to a restaurant application and the third one to an auditorium application. Each case study was carried out for an occupancy ratio and three ventilation categories (I, II and III). The values of occupancy ratio and volumetric air flow rate for each ventilation category were taken from the European ventilation standard (EN-16798–1, 2019; EN-16798–2, 2019). The ventilation air flow rate requirements for the DIEC system are shown in Table 4.

The type of space to be air-conditioned, the outdoor air conditions and the supply air conditions of the DIEC system were set constant to carry out the case studies. These parameters are summarized in Table 5. Other case studies with different outdoor air conditions and different supply air conditions were also carried out. Nevertheless, the optimal design and performance of the DIEC were similar to those shown in the present work, so these results were not included for reasons of clarity and space in the paper. The values of area ratio, person ratio and CO_2 generation rate were given by the European ventilation standard (EN-16798–1, 2019; EN-16798–2, 2019).

The optimal geometric design and optimal operational parameters were evaluated in terms of the compactness of the DIEC system, C_{DIEC}, and coefficient of performance, COP. Such ratios were defined by Eqs. (25) and (26), respectively. C_{DIEC} was analysed with a ratio, in order to evaluate the cooling capacity, $\dot{Q}_{cool}$, that led the lowest volume, Vol, of the DIEC system. $\dot{Q}_{cool}$ represents the sensible energy delivered by the DIEC system and Vol was obtained with the length, width and height of the exchange module.

$$C_{DIEC} = \frac{\dot{Q}_{cool}}{Vol} \tag{25}$$

$$COP = \frac{\dot{Q}_{cool}}{\dot{W}} \tag{26}$$

3. Results

3.1. Experimental results

The experimental tests N1-N21 were used to evaluate the variation of process air temperature, ΔT, and of dew point effectiveness, ε_{dp}, by varying T_{in} and $\dot{V}_{in}$ under different R values. The results of ΔT and ε_{dp} for two inlet air temperature values, 32 °C and 42 °C, two inlet air flow rate, 3500 $m^3 h^{-1}$ and 4500 $m^3 h^{-1}$, and seven R values, 0.2 to 0.8, are shown in Fig. 3. It can be observed than the values of ΔT and ε_{dp} increased when the R values were raised. In addition, asymptotic trends of ΔT and ε_{dp} are shown as R increased, regardless of the variation of T_{in} and $\dot{V}_{in}$. The highest values of ΔT and ε_{dp} were obtained for R equal to 0.8 and the lowest values of ΔT and ε_{dp} were obtained for R equal to 0.2, see Fig. 3.

Regarding T_{in}, the ΔT values were always higher for T_{in} equal to 42 °C with respect to T_{in} equal to 32 °C, see Fig. 3a. The ε_{dp} values were also

Table 4
Case studies.

Occupancy ratio [person m^{-2}]	Ventilation requirements according to the European ventilation standard. Volumetric air flow rate [$m^3 h^{-1}$]		
	Category I(20 l s^{-1} person^{-1})	Category II(14 l s^{-1} person^{-1})	Category III(8 l s^{-1} person^{-1})
0.1 (Office)	720	504	288
0.7 (Restaurant)	5040	3528	2016
1.4 (Auditorium)	108,000	7560	4320

Table 5
Characteristics of the building, the outdoor air conditions and the supply air conditions.

Building	Value
Area	100 m^2
Area ratio	0.7 l s^{-1} m^{-2}
Person ratio	7 l s^{-1} person^{-1}
CO_2 generation rate	20 l h^{-1} person^{-1}
Outdoor air conditions	
Temperature	40 °C
Humidity ratio	9 g kg^{-1}
CO_2 concentration	400 ppm
Supply air conditions	
Temperature	18 °C
Humidity ratio	9 g kg^{-1}

higher for T_{in} equal to 42 °C and low R values, see Fig. 3b. Nevertheless, the ε_{dp} values were similar for both T_{in} and medium and high R values. The maximum values of ΔT and ε_{dp} were 32.8 °C and 0.87, respectively, for T_{in} equal to 42 °C and R equal to 0.8.

The trend of the inlet air flow rate, $\dot{V}_{in}$, with respect to different R values has also been analysed in terms of ΔT and ε_{dp}, as shown in Fig. 3. Comparing the results obtained for both air flow rate values, it can be seen than the values of ΔT and ε_{dp} were always higher for $\dot{V}_{in}$ equal to 3500 $m^3 h^{-1}$ than those for $\dot{V}_{in}$ equal to 4500 $m^3 h^{-1}$. The variation of ΔT and ε_{dp} for both $\dot{V}_{in}$ values was maximum when the R value was increased, 7 °C and 0.1, respectively, for R equal to 0.8. The ε_{dp} uncertainty values of some case studies were within other ε_{dp} uncertainty values. So, the ε_{dp} differences for the case studies with the same R value was not always guaranteed, see Fig. 3b.

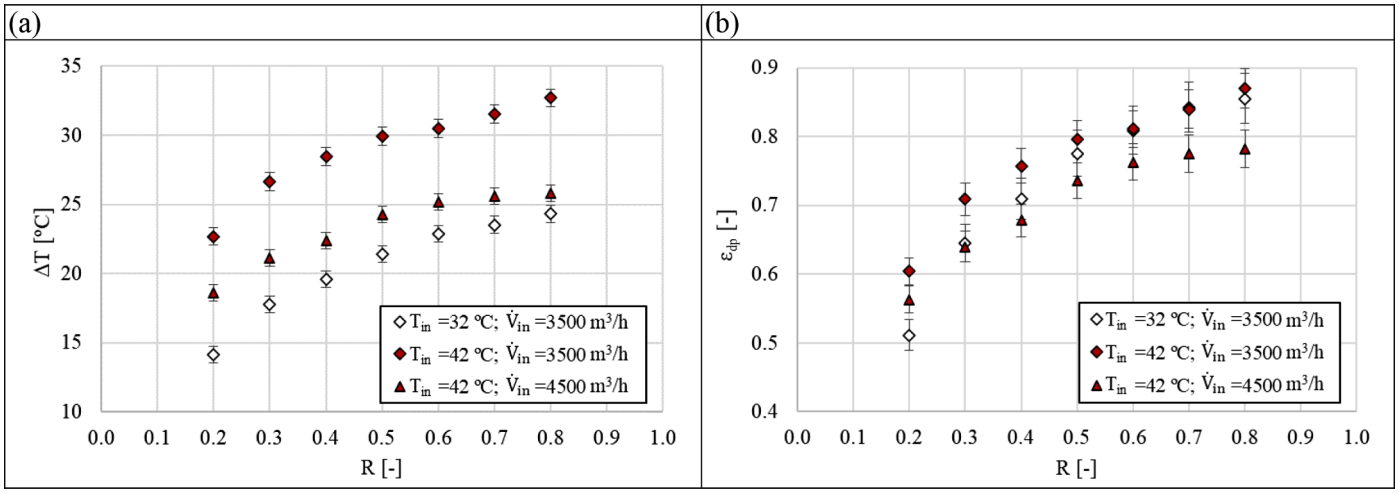

Fig 3. Variation of process air temperature and of dew point effectiveness for the experimental tests N1-N21.

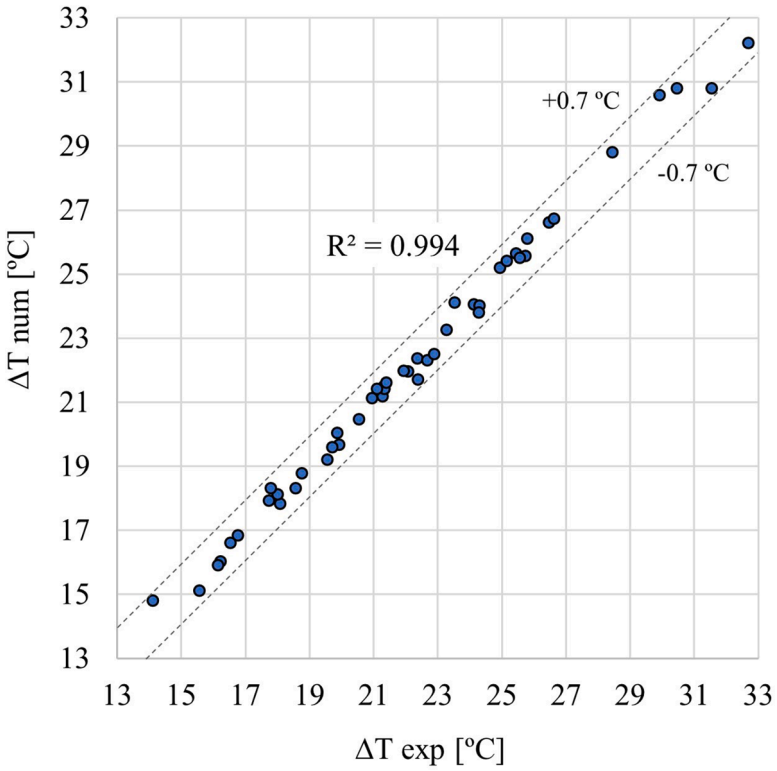

Fig 4. Parity plot of the experimental and numerical ΔT results of the dew-point indirect evaporative cooler.

These experimental results show that for a R value of 0.8 and a low air flow rate of 3500 $m^3\ h^{-1}$, the studied air-cooling system allowed to achieve supply air conditions very close to dew point conditions, regardless of the T_{in} value.

3.2. Validation of the detailed mathematical model

The experimental results obtained from tests N1-N50, see Table 3, have been compared with the numerical results obtained with the mathematical DIEC model described in Section 2.3. The values of variation of process air temperature, ΔT, were used for this comparative analysis. As shown in Fig. 4, there was a very good agreement between numerical and experimental process air temperature variation, being the deviation always within 0.7 °C, and a R^2 value equal to 0.994. Therefore, this detailed mathematical model can be used to analyse DIEC.

3.3. Analysis of design and performance

In the present work, the optimal geometric design and the optimal operational parameters of DIEC to be able to achieve cooling conditions and comply with the European ventilation regulations (EN-16798–1, 2019) were studied.

3.3.1. Analysis of length and the energy consumption

The trends of the length, L_{DIEC}, and the energy consumption, $\dot{W}$, of DIEC have been preliminary analysed by varying $\dot{V}_{SA}$, and R, in order to obtain a deeper understanding of the behaviour of the DIEC, see Fig. 5-Fig. 6.

In Fig. 5, the remaining input variables were fixed at constant values: T_{in}=40 °C; ω_{in}=9 g kg^{-1}; $R = 0.5$. The values of supply air temperature and humidity ratio were also fixed at constant values, 18 °C and 9 g kg^{-1}, as described in Section 2.4. The supply air flow rate, $\dot{V}_{SA}$, was directly related to the cooling capacity, $\dot{Q}_{cool}$, because the inlet and outlet air conditions were set constant. It can be observed than the L_{DIEC} values increased when the $\dot{V}_{SA}$ value was raised, since $\dot{Q}_{cool}$ must also be greater. The length trend obtained was linear. In addition, the increase in $\dot{V}_{SA}$ caused the inlet and exhaust air flow rates ($\dot{V}_{in}$ and $\dot{V}_{EA}$) to also increase, thus increasing the air velocities in the channels. The increase in air velocity and length caused an increase in $\dot{W}$, see Fig. 5, mainly due to the increase in pressure drop in the channels. The $\dot{W}$ output was not linear when varying $\dot{V}_{SA}$.

The results of L_{DIEC} and $\dot{W}$ of DIEC for different R values are shown in Fig. 6. The inlet air conditions for this case study were set at: T_{in}=40 °C; ω_{in}=9 g kg^{-1}; $\dot{V}_{in}$=5000 $m^3\ h^{-1}$. It is highlighted that the higher R, the higher percentage of air flow rate was exhausted. In addition, the higher R, the lower $\dot{Q}_{cool}$, since the supply air flow rate, $\dot{V}_{SA}$, decreased and the inlet and outlet air conditions were set constant in this analysis. This trend was inverse to that reached in Fig. 5.

In Fig. 6, it can be observed than the L_{DIEC} value decreased to reach the required supply air conditions when the R values increased, because $\dot{V}_{SA}$ decreased. The L_{DIEC} variation was more significant for low R values, where $\dot{V}_{SA}$ was higher and, therefore, $\dot{Q}_{cool}$ was also higher. This trend was due to the fact that the length was related to the value of the air velocity squared.

The W trend show in Fig. 6 was due to the pressure drops generated in the primary channels, in the secondary channels and in the air supply. These pressure drops are represented in Fig. 7. The total pressure drop of DIEC was the sum of these three. The pressure drop in the primary channels, ΔPp, was always constant for different R values. The pressure drop of the air supply, ΔPSA, increased and the pressure drop of the secondary channels decreased, ΔPs, when the R value was reduced, see Fig. 7. However, the ΔPSA value outweighed the ΔPs value, reaching an increase in W for low R values, as shown in Fig. 6. These trends were mainly due to supply and return air velocities. For high R values the trends of pressure drops and W were inverse, see Fig. 6-Fig. 7. The maximum W value was reached for R equal to 0.2, as shown in Fig. 6, and the minimum W value coincided at the equilibrium point of the curves of ΔPSA and ΔPs.

3.3.2. Analysis of the case studies

Three case studies were carried out in order to analyse the optimal design and performance of DIEC, as discussed in Section 2.4: office application, restaurant application and auditorium application. The case studies were carried out for different operation modes, analysing C_{DIEC}, and COP.

- Office application (occupancy ratio= 0.1 person m^{-2})

The results of C_{DIEC} and COP for the office application are shown in Fig. 8. These results were obtained for different values of R and $\dot{V}_{SA}$ (or $CO_{2,ind}$). It can be observed than the trend of C_{DIEC} was parabolic, when $\dot{V}_{SA}$ remained constant, see Fig. 8a. The highest compactness of the

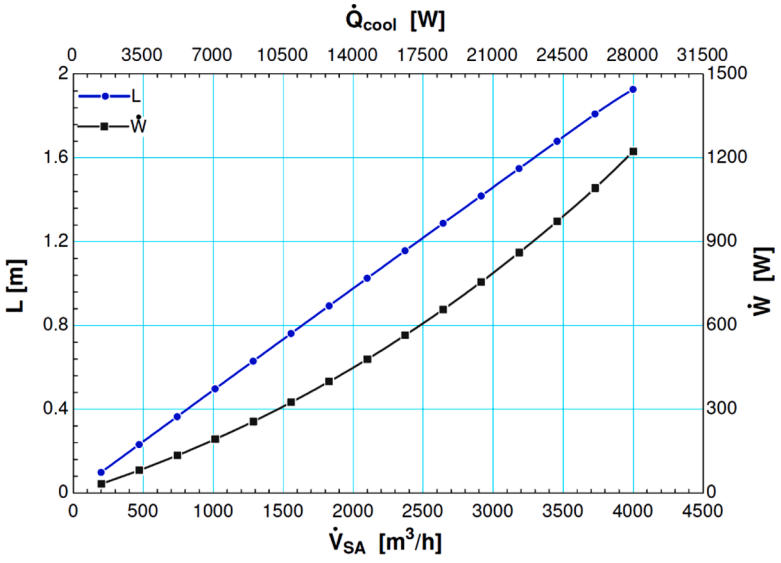

Fig 5. Length and the energy consumption of the dew-point indirect evaporative cooler for different values of supply air flow rate (constant values: T_{in}=40 °C; ω_{in}=9 g kg^{-1}; $R = 0.5$).

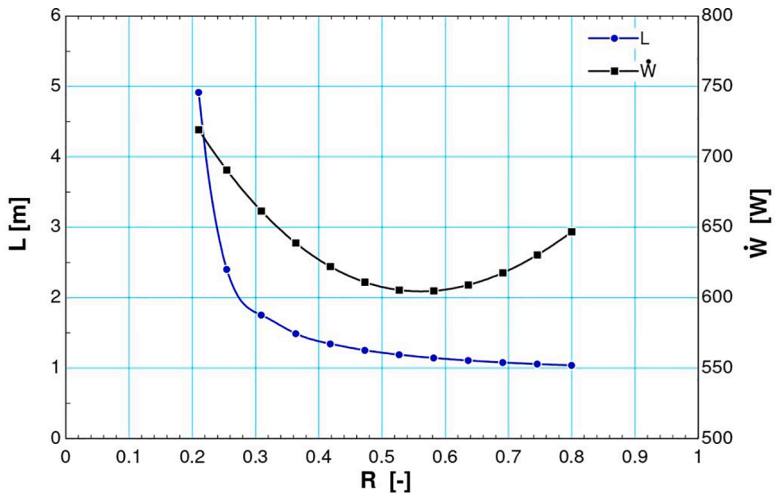

Fig 6. Length and the energy consumption of the dew-point indirect evaporative cooler for different values of R (constant values: T_{in}=40 °C; ω_{in}=9 g kg^{-1}; $\dot{V}_{in}$=5000 $m^3\ h^{-1}$).

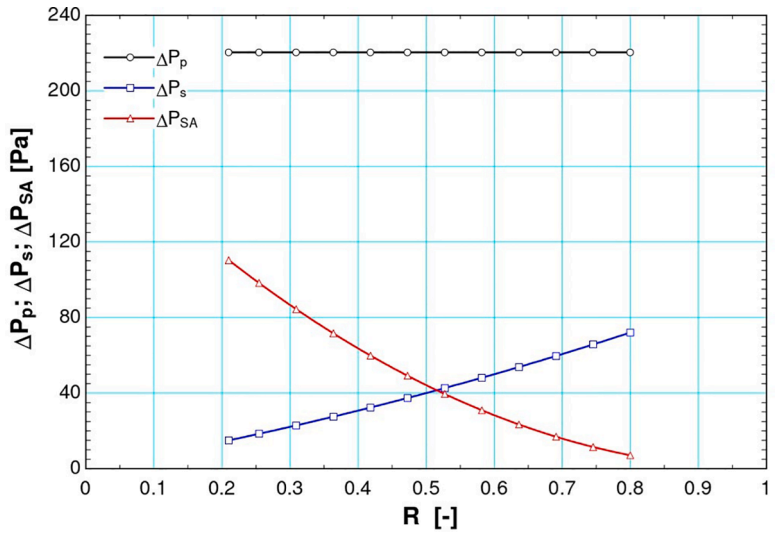

Fig 7. Pressure drops of the dew-point indirect evaporative cooler (constant values: T_{in}=40 °C; ω_{in}=9 g kg^{-1}; $\dot{V}_{in}$=5000 $m^3\ h^{-1}$).

device was achieved for R values equal to 0.45, 16,632 W m^{-3} for values of $\dot{Q}_{cool}$ and Vol of 4974 W and 0.3 m^3, respectively. However, the compactness was reduced for R values lower and higher than this inflection point, achieving a minimum C_{DIEC} value for R equal to 0.2. C_{DIEC} increased up to 76% when using an R value of 0.45 instead of an R value of 0.2. Regarding $\dot{V}_{SA}$, both $\dot{Q}_{cool}$ and Vol increased when $\dot{V}_{SA}$ increased and R remained constant, however, the increase in $\dot{Q}_{cool}$ was slightly larger than the increase in Vol, see Eq. (25). Therefore, the C_{DIEC} values increased slightly when $\dot{V}_{SA}$ was increased, see Fig. 8a.

The COP values increased when R was reduced and $\dot{V}_{SA}$ remained constant, see Fig. 8b. This fact was due to the reduction of $\dot{V}_{EA}$ and $\dot{W}$. On the other hand, for constant R values, COP was slightly reduced when $\dot{V}_{SA}$ was increased, see Fig. 8b. Therefore, the increase in $\dot{W}$was greater than that of $\dot{Q}_{cool}$. The maximum COP value was 50.26 for R equal to 0.2 and $\dot{V}_{SA}$ equal to 288 $m^3\ h^{-1}$. The COP value increased up to 75% when using an R value of 0.2 instead of an R value of 0.8. Furthermore, it can be seen that the optimal C_{DIEC} and COP values were obtained for different working conditions, so a detailed analysis of the optimal conditions was carried out at the end of Section 3.3.2.

- Restaurant application (occupancy ratio= 0.7 person m^{-2})

The results of the restaurant application are shown in Fig. 9. A difference between this case study and the office application was the $\dot{V}_{SA}$ values, which were significantly higher to reach the ventilation categories I, II and III, see Table 4.

It can be observed that the trends of C_{DIEC} and COP reported in Fig. 9 for low $\dot{V}_{SA}$ values were similar to those of the office application. The C_{DIEC} values increased significantly when $\dot{V}_{SA}$ increased and the R values were high and remained constant, see Fig. 9a. This trend was due to the increase in $\dot{Q}_{cool}$.and the reduction in Vol. The trend of C_{DIEC} was different when $\dot{V}_{SA}$ increased and the R values were low and remained constant, since the variation of $\dot{Q}_{cool}$ and Vol was similar. The maximum C_{DIEC} value was achieved for values of R and $\dot{V}_{SA}$ equal to 0.75 and 5040 $m^3\ h^{-1}$, respectively, 25,195 W m^{-3}, see Fig. 9a. Therefore, the optimal DIEC design for the considered conditions was achieved for high values of $\dot{V}_{SA}$ and R.

Regarding COP, it can be seen that the DIEC system increased its performance for low R values, $\dot{V}_{SA}$ remained constant, see Fig. 9b. The COP value increased up to 87% when using an R value of 0.2 instead of

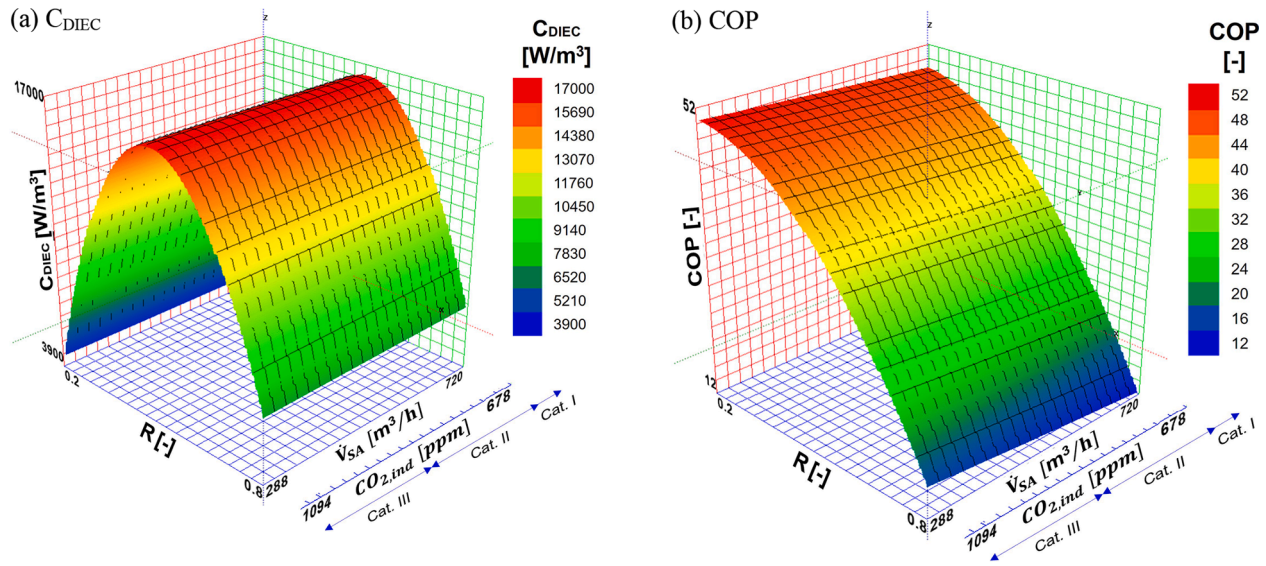

Fig. 8. Results of compactness and coefficient of performance of the DIEC system for the office application.

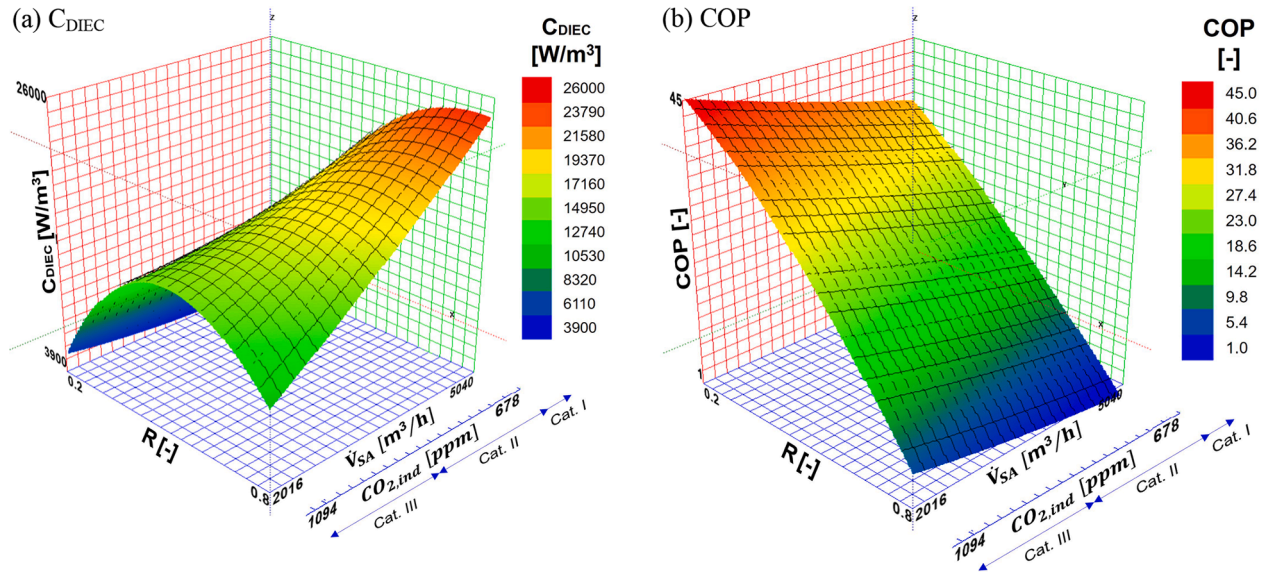

Fig 9. Results of compactness and coefficient of performance of the DIEC system for the restaurant application.

an R value of 0.8. COP also improved for low $\dot{V}_{SA}$ values, mainly due to the reduction of $\dot{W}$ with low $\dot{V}_{SA}$ values, achieving a maximum COP value of 44.19 for R and $\dot{V}_{SA}$ equal to 0.2 and 2016 $m^3\,h^{-1}$, respectively.

- Auditorium (Occupancy ratio: 1.4 person m^{-2})

The trends of C_{DIEC} and COP for the auditorium application were similar to those of the restaurant application, see Fig. 10. It is highlighted that for low R values, a higher variation of C_{DIEC} and COP was obtained when $\dot{V}_{SA}$ was modified, due to a higher ventilation requirement to reach categories I, II and III.

For the three case studies, the optimal design and performance of DIEC were achieved in different operating states, even in opposite states as shown in Fig. 9 and Fig. 10. Therefore, an optimal DIEC design could be considered when the maximum values of C_{DIEC} and COP are obtained at the same time for a considered operating condition. These operating states where both ratios intersect for the three applications were represented in Fig. 11. For example, for the restaurant application (occupancy ratio= 0.7 person m^{-2}) with a flow rate of 5040 m3/h (Category I), the maximum values of C_{DIEC} and COP were obtained for an R value of 0.75 and 0.2, respectively, see Fig. 9. Therefore, the optimal values of both parameters were obtained for different R values. With the methodology described, the optimal DIEC design was found for the R value where the values of C_{DIEC} and COP intersected in the surface curve. In this case, an R value of 0.31 was found for a COP of 29.7 and C_{DIEC} of 15,728 W m^{-3}.

In Fig. 11, it can be observed that the operating states of DIEC for the office application (0.1 person m^{-2}) were always obtained for a R value close to 0.35, regardless of the variation of $\dot{V}_{SA}$. The COP values were approximately 46 and the C_{DIEC} values were approximately 16,580 W m^{-3} for all states. For the restaurant application (0.7 person m^{-2}), the operating states were obtained for R values between 0.3 and 0.37. These operating states were reduced from Category III to Category I, i.e., when $\dot{V}_{SA}$ increased, see Fig. 11. For this case study, the C_{DIEC} values varied from 15,728 W m^{-3} (category I) to 16,799 W m^{-3} (category III). Finally, for the auditorium application (1.4 person m^{-2}), the operating states of DIEC varied with R, between 0.2 and 0.4, for each category, see Fig. 11.

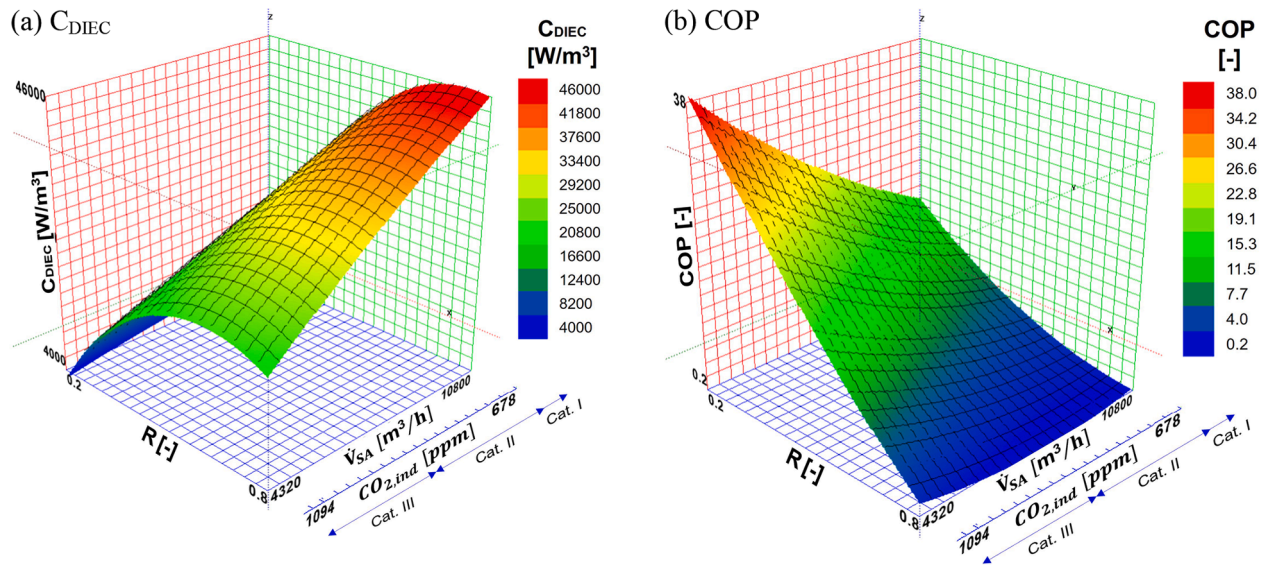

Fig 10. Results of compactness and coefficient of performance of the DIEC system for the auditorium application.

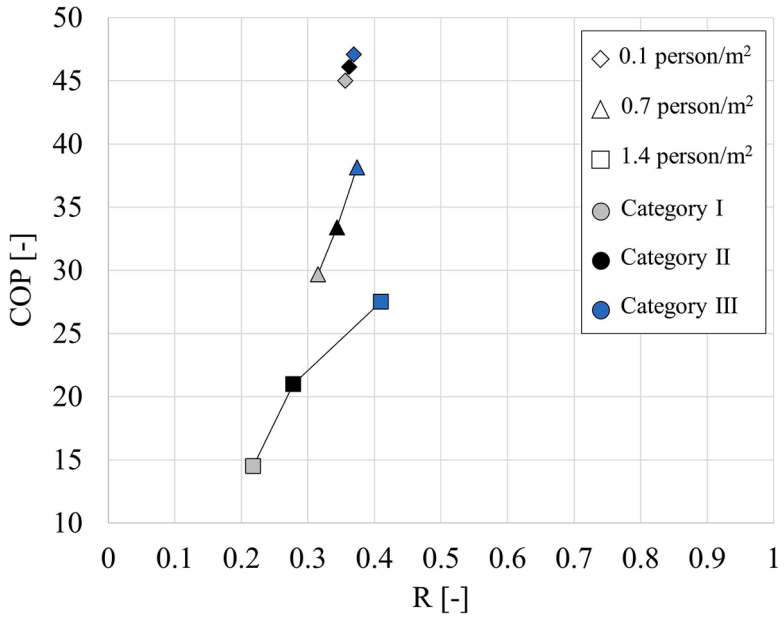

Fig 11. Operating states where compactness and coefficient of performance intersect.

The COP values varied between 14.5 and 27.5 and the C_{DIEC} values varied between 12,757 W m^{-3} and 17,048 W m^{-3} for the auditorium application.

The results showed that an DIEC with high COP values and a compact geometric design can be obtained for buildings with different applications, achieving indoor cooling conditions and complying with the European ventilation regulations (EN-16798–1, 2019).

3.4. Limitations of this study

Based on the results shown, a wide range of performance values and optimal designs have been obtained. The results obtained are valid for the dimensions and materials of the channels shown in Table 1. On the other side, in the studied range of operating conditions, the mathematical model developed adequately predicts the experimental operating conditions of DIEC units. A new validation study would be necessary for operational conditions outside this range. Moreover, the mathematical model of DIEC is valid under five assumptions, which were indicated in Section 2.3.

4. Conclusions

In the present work, dew-point indirect evaporative cooling, DIEC, systems were analysed experimentally and numerically. The optimal geometric design and operational parameters of DIEC systems to achieve cooling conditions and comply with the European ventilation regulations were obtained for three case studies: office application, restaurant application and auditorium application.

The experimental results showed that for high R (ratio of exhaust air flow rate to inlet air flow rate) values and low inlet air flow rates, the DIEC system allowed to achieve supply air conditions very close to dew-point conditions, regardless of the inlet air temperature value.

The results of the optimal geometric design and operational parameters of DIEC depended on the type of space to be air-conditioned and

the ventilation category indicated in the EN 16,798 European Standard. For the office application, the optimal DIEC design was always obtained for R values equal to 0.45 for the three ventilation categories. However, for the restaurant and auditorium applications, the optimal design varied for different R values, between 0.45 and 0.8, depending on the ventilation category.

The optimal DIEC performance was always obtained for low R values, 0.2, for the three ventilation categories, with COP values up to 50.26 for the office application, 44.19 for the restaurant application and 37.14 for the auditorium application. This fact was mainly due to the reduction of energy consumption of the DIEC systems when they work with low R values.

These results showed that an DIEC with high performance values and a compact geometric design can be obtained for buildings with different applications, achieving indoor cooling conditions and complying with the European ventilation regulations.

Declaration of Competing Interest

Manuscript title: Experimental and numerical study of dew-point indirect evaporative coolers to optimize performance and design The authors certify that: We have no conflict of interest to declare.

Acknowledgement

The authors acknowledge the financial support received by the European Regional Development Fund and the Andalusian Economy, Knowledge, Enterprise and University Council, Spain, through the research project HICOOL, reference 1263034, and by European Union's Horizon 2020 research and innovation programme, through the research project WEDISTRICT, reference H2020-WIDESPREAD2018–03–857801. Funding for open access charge: Universidad de Córdoba / CBUA.

Supplementary materials

Supplementary material associated with this article can be found, in the online version, at doi:10.1016/j.ijrefrig.2022.06.006.

References

Ali, M., Ahmad, W., Sheikh, N.A., Ali, H., Kousar, R., Rashid ur, T., 2020. Performance enhancement of a cross flow dew point indirect evaporative cooler with circular finned channel geometry. J. Build. Eng. 101980 https://doi.org/10.1016/j.jobe.2020.101980.

Comino, F., Castillo González, J., Navas-Martos, F.J., Ruiz de Adana, M., 2020. Experimental energy performance assessment of a solar desiccant cooling system in Southern Europe climates. Appl. Therm. Eng. 165 https://doi.org/10.1016/j.applthermaleng.2019.114579.

Comino, F., Guijo-Rubio, D., Ruiz de Adana, M., Hervás-Martínez, C., 2019. Validation of multitask artificial neural networks to model desiccant wheels activated at low temperature. Int. J. Refrig. 100 https://doi.org/10.1016/j.ijrefrig.2019.02.002.

Comino, F., Milani, S., De Antonellis, S., Joppolo, C.M., Ruiz de Adana, M., 2018a. Simplified performance correlation of an indirect evaporative cooling system: development and validation. Int. J. Refrig. 88, 307–317. https://doi.org/10.1016/j.ijrefrig.2018.02.002.

Comino, F., Ruiz de Adana, M., Peci, F., 2018b. Energy saving potential of a hybrid HVAC system with a desiccant wheel activated at low temperatures and an indirect evaporative cooler in handling air in buildings with high latent loads. Appl. Therm. Eng. 131, 412–427. https://doi.org/10.1016/j.applthermaleng.2017.12.004.

Duan, Z., Zhao, X., Li, J., 2017. Design, fabrication and performance evaluation of a compact regenerative evaporative cooler: towards low energy cooling for buildings. Energy 140, 506–519. https://doi.org/10.1016/j.energy.2017.08.110.

EN-16798-1, 2019. Energy performance of buildings - Ventilation for buildings - Part 1: indoor environmental input parameters for design and assessment of energy performance of buildings addressing indoor air quality, thermal environment, lighting and acoustics.

EN-16798-2, 2019. Energy performance of buildings - Ventilation for buildings - Part 2: interpretation of the requirements in EN 16798-1.

Guilizzoni, M., Milani, S., Liberati, P., De Antonellis, S., 2019. Effect of plates coating on performance of an indirect evaporative cooling system. Int. J. Refrig. 104, 367–375. https://doi.org/10.1016/j.ijrefrig.2019.05.029.

Hasan, A., 2012. Going below the wet-bulb temperature by indirect evaporative cooling: analysis using a modified ε-NTU method. Appl. Energy 89, 237–245. https://doi.org/10.1016/j.apenergy.2011.07.005.

IEA, 2018. The future of cooling.

Jafarian, H., Sayyaadi, H., Torabi, F., 2017. A numerical model for a dew-point counter-flow indirect evaporative cooler using a modified boundary condition and considering effects of entrance regions. Int. J. Refrig. 84, 36–51. https://doi.org/10.1016/j.ijrefrig.2017.09.003.

Klein, S.A., 2020. Enginering Equation Solver (EES). F-Chart Softw, Madison, WI.

Lin, J., Bui, D.T., Wang, R., Chua, K.J., 2018. The counter-flow dew point evaporative cooler: analyzing its transient and steady-state behavior. Appl. Therm. Eng. 143, 34–47. https://doi.org/10.1016/j.applthermaleng.2018.07.092.

Lin, J., Wang, R.Z., Kumja, M., Bui, T.D., Chua, K.J., 2017. Modelling and experimental investigation of the cross-flow dew point evaporative cooler with and without dehumidification. Appl. Therm. Eng. 121, 1–13. https://doi.org/10.1016/j.applthermaleng.2017.04.047.

Oh, S.J., Shahzad, M.W., Burhan, M., Chun, W., Kian Jon, C., KumJa, M., Ng, K.C., 2019. Approaches to energy efficiency in air conditioning: a comparative study on purge configurations for indirect evaporative cooling. Energy 168, 505–515. https://doi.org/10.1016/j.energy.2018.11.077.

Pandelidis, D., Anisimov, S., 2016. Application of a statistical design for analyzing basic performance characteristics of the cross-flow Maisotsenko cycle heat exchanger. Int. J. Heat Mass Transf. 95, 45–61. https://doi.org/10.1016/j.ijheatmasstransfer.2015.11.060.

Pandelidis, D., Anisimov, S., Drag, P., 2017. Performance comparison between selected evaporative air coolers. Energies 10, 1–20. https://doi.org/10.3390/en10040577.

Pandelidis, D., Cichoń, A., Pacak, A., Drąg, P., Drąg, M., Worek, W., Cetin, S., 2020. Performance study of the cross-flow Maisotsenko cycle in humid climate conditions. Int. Commun. Heat Mass Transf. 115, 104581 https://doi.org/10.1016/j.icheatmasstransfer.2020.104581.

Ren, C., Yang, H., 2006. An analytical model for the heat and mass transfer processes in indirect evaporative cooling with parallel/counter flow configurations. Int. J. Heat Mass Transf. 49, 617–627. https://doi.org/10.1016/j.ijheatmasstransfer.2005.08.019.

Romero-lara, M.J., Comino, F., de Adana, M.R., 2021. Seasonal analysis comparison of three air-cooling systems in terms of thermal comfort, air quality and energy consumption for school buildings in mediterranean climates. Energies 14. https://doi.org/10.3390/en14154436.

Sadighi Dizaji, H., Hu, E.J., Chen, L., 2018a. A comprehensive review of the Maisotsenko-cycle based air conditioning systems. Energy 156, 725–749. https://doi.org/10.1016/j.energy.2018.05.086.

Sadighi Dizaji, H., Hu, E.J., Chen, L., Pourhedayat, S., 2019. Using novel integrated Maisotsenko cooler and absorption chiller for cooling of gas turbine inlet air. Energy Convers. Manag. 195, 1067–1078. https://doi.org/10.1016/j.enconman.2019.05.064.

Sadighi Dizaji, H., Hu, E.J., Chen, L., Pourhedayat, S., 2018b. Development and validation of an analytical model for perforated (multi-stage) regenerative M-cycle air cooler. Appl. Energy 228, 2176–2194. https://doi.org/10.1016/j.apenergy.2018.07.018.

Shahzad, M.W., Burhan, M., Ybyraiymkul, D., Oh, S.J., Ng, K.C., 2019. An improved indirect evaporative cooler experimental investigation. Appl. Energy 256, 113934. https://doi.org/10.1016/j.apenergy.2019.113934.

Shahzad, M.W., Lin, J., Xu, B.Bin, Dala, L., Chen, Q., Burhan, M., Sultan, M., Worek, W., Ng, K.C., 2021. A spatiotemporal indirect evaporative cooler enabled by transiently interceding water mist. Energy 217, 119352. https://doi.org/10.1016/j.energy.2020.119352.

Sohani, A., Farasati, Y., Sayyaadi, H., 2017. A systematic approach to find the best road map for enhancement of a power plant with dew point inlet air pre-cooling of the air compressor. Energy Convers. Manag. 150, 463–484. https://doi.org/10.1016/j.enconman.2017.08.028.

Sohani, A., Sayyaadi, H., Hoseinpoori, S., 2016. Modeling and multi-objective optimization of an M-cycle cross-flow indirect evaporative cooler using the GMDH type neural network. Int. J. Refrig. 69, 186–204. https://doi.org/10.1016/j.ijrefrig.2016.05.011.

Wang, C.C., Prather, K.A., Sznitman, J., Jimenez, J.L., Lakdawala, S.S., Tufekci, Z., Marr, L.C., 2021. Airborne transmission of respiratory viruses. Science (80-.). 373, eabd9149. https://doi.org/10.1126/science.abd9149.